Protection of LVDC Microgrids in Grid-Connected and Islanded Modes Using Bifurcation Theory

Ahmadi, Sima; Sadeghkhani, Iman; Shahgholian, Ghazanfar; Fani, Bahador; Guerrero, Josep M.

Published in:
IEEE Journal of Emerging and Selected Topics in Power Electronics

DOI (link to publication from Publisher):
10.1109/JESTPE.2019.2961903

Publication date:
2021

Document Version
Accepted author manuscript, peer reviewed version

This article has been accepted for publication in a future issue of this journal, but has not been fully edited. Content may change prior to final publication. Citation information: DOI 10.1109/JESTPE.2019.2961903, IEEE Journal of Emerging and Selected Topics in Power Electronics

Protection of LVDC Microgrids in Grid-Connected and Islanded Modes Using Bifurcation Theory

Sima Ahmadi, Iman Sadeghkhani, Ghazanfar Shahgholian, Bahador Fani, and Josep M. Guerrero, *Fellow, IEEE*

***Abstract*—Low voltage DC (LVDC) microgrids facilitate the integration of renewable energy systems and modern loads. However, they suffer from the lack of a sensitive, selective, reliable, and fast protection strategy. The low fault current of high-resistance faults makes fault detection and faulty zone identification challenging tasks for protection engineers. This paper proposes a protection scheme that is effective for both bolted and high-resistance faults at LVDC feeders. The developed strategy relies on two intelligent electronic devices at both ends of the protected zone, calculating the normalized superimposed component of the line current. By adding this component to the input of the periodically-forced harmonic oscillator (PFHO), both fault occurrence and fault direction can be simultaneously determined based on the oscillator state variable with only two possible values during stable and unstable modes. It eliminates the need for selection of various protection thresholds for different LVDC microgrid structures/topologies. The proposed protection strategy can classify pole-to-ground and pole-to-pole faults and is effective for both grid-connected and islanded LVDC microgrids. The reliable performance of the developed PFHO based protection is assessed on the simulation model of a $\pm$750 V meshed LVDC microgrid with the TN-S grounding system.**

***Index Terms*—Fault detection, directional protection, harmonic oscillator, high-resistance fault, low voltage DC microgrid.**

I. Introduction

ONE of the main technical challenges of low voltage DC (LVDC) microgrids that remains unsolved is to develop a protection system with acceptable sensitivity, selectivity, reliability, and speed [1], [2]. DC microgrids are prone to both pole-to-ground (PG) and pole-to-pole (PP) faults. The high fault current magnitude and rate of change caused by capacitor discharge make the protection requirements of DC microgrid different from those of AC microgrids. Also, the conventional AC circuit breakers are ineffective in DC microgrids due to the need for the high-speed current interruption and no zero-crossing point. The limited fault current of converters and short lines are other protection challenges of DC microgrids.

Various protection schemes proposed for DC microgrids can be broadly classified into two categories: (i) non-unit protection schemes and (ii) unit protection schemes.

Category I–Non-Unit Protection Schemes: Distance protection, overcurrent protection, and current derivative protection are the main groups of this category.

- Distance Protection: Using voltage reference comparison, [3] measures the distance to the fault point while the ground faults are located using ground resistance and distance to the fault estimations by circuit analysis. The distance protection scheme proposed in [4] measures the apparent instantaneous resistance using converter voltage and current. The low protection speed is the main disadvantage of this group.
- Overcurrent Protection: Similar to the conventional protection system of distribution networks, the overcurrent protection is proposed for DC microgrids. Ref. [5] presents an overcurrent based protection strategy for multiterminal DC distribution networks. Using passive elements and current and voltage transducers, [6] presents a hybrid passive overcurrent relay for DC microgrids which can detect high-resistance faults by employing both real-time discrete wavelet transform and overcurrent function. However, these schemes suffer from low sensitivity or need for extra devices.
- Current Derivative Protection: The protection scheme proposed in [7] is based on the line current derivative while employing DC current natural characteristics and its first and second derivatives are the basis of the protection scheme proposed in [8]. Susceptibility to noise is the main disadvantage of this group.

Category II–Unit Protection Schemes: The bidirectional fault current of looped/meshed microgrids commonly makes the non-unit protection schemes ineffective. To address this problem, the unit protection is commonly used that the differential and directional protections are its main groups.

- Differential Protection: The differential protection that compares the current at both ends of the protected zone is proposed in [9], [10]. Modified cumulative sum average methods are employed in differential protection schemes proposed in [11], [12]. However, differential protection suffers from the need for synchronization.
- Directional Protection: The operating principle of directional protection is current direction change during the fault condition in only one end of the faulty zone. Using the current direction information at protected zone ends, [13] presents a directional protection scheme for DC microgrids. The fault direction information in [14] is determined by the least square method based fault path parameter estimation. Using the oscillation frequency and transient power information at both ends, [15] detects and locates the fault, respectively. However, when the fault path resistance is high, the current direction does not change, making directional protection ineffective. To address this problem, the superimposed component based directional protection schemes have recently gained

S. Ahmadi, I. Sadeghkhani, G. Shahgholian, and B. Fani are with the Department of Electrical Engineering, Najafabad Branch, Islamic Azad University, Najafabad 85141-43131, Iran (email: s.ahmadi@sel.iaun.ac.ir, sadeghkhani@pel.iaun.ac.ir (corresponding author), shahgholian@iaun.ac.ir, b.fani@pel.iaun.ac.ir).

J. M. Guerrero is with the Institute of Energy Technology, Aalborg University, Aalborg 9220, Denmark (email: joz@et.aau.dk).

This article has been accepted for publication in a future issue of this journal, but has not been fully edited. Content may change prior to final publication. Citation information: DOI 10.1109/JESTPE.2019.2961903, IEEE Journal of Emerging and Selected Topics in Power Electronics

popularity among researchers. In [16], a superimposed current based directional protection is proposed while in [17], the superimposed component of transient energy is used in directional protection. The directional protection scheme proposed in [18] is based on the modified squared poverty gap (MSPG) index calculated using the superimposed component of current.

The unit protection schemes suffer from two problems: (1) their reliable operation depends on the proper selection of the fault detection threshold that its value may not be the same for different microgrid structures/topologies and (2) they are evaluated for either a grid-connected (most of them) or an islanded DC microgrid. To address these problems, this paper presents a superimposed component based unit protection for feeders of meshed LVDC microgrids. In the proposed protection strategy, each protected zone is equipped with two intelligent electronic devices (IEDs) to calculate the superimposed component of the line current at both ends. This component is added to the input of the periodically-forced harmonic oscillator (PFHO). The main feature of the proposed PFHO based protection scheme is that by monitoring the PFHO state variable, the fault occurrence and fault direction are determined simultaneously without the need for the threshold calculation because independent of microgrid structure/topology, this variable is either smaller than two for the normal operation/forward fault or infinity for the reverse fault. The proposed scheme can detect high-resistance faults and is evaluated in both grid-connected and islanded microgrids. Also, unlike the conventional unit protection of AC networks, it can classify PG and PP faults.

The rest of the paper is organized as follows. Section II presents the proposed PFHO based protection algorithm. The test meshed LVDC microgrid network and control structure of DC and AC converters are described in Section III. Section IV is dedicated to evaluating the performance of the proposed strategy. Finally, Section V concludes the paper.

II. Proposed Methodology

The meshed LVDC microgrid requires an effective protection system, addressing the bidirectional and low amplitude fault current during high-resistance faults without the need for threshold selection and with the proper performance in both grid-connected and islanded modes of operation. To this end, this paper proposes a unit protection system using the bifurcation theory that can effectively detect the weak signals.

A. Bifurcation Theory

1) Hyperbolic Equilibrium Points in Continuous-Time Systems: Consider a continuous-time parameter-dependent dynamic system as [19]

$$\dot{x} = f(x, \alpha), \tag{1}$$

where $x \in \mathbb{R}^n$ and $\alpha \in \mathbb{R}^m$ are the state variables and set parameters, respectively, and f is a smooth function. Assume that $x_0 = 0$ is an equilibrium point of system ($f(x_0) = 0$) and $\mathbf{A}$ is the Jacobian matrix df/dx calculated at x_0. Also, n_-, n_0, and n_+ are the number of $\mathbf{A}$ eigenvalues with negative, zero, and positive real values, respectively. If $n_0 = 0$, the equilibrium point is hyperbolic (no eigenvalue at imaginary axis) and if $n_- n_+ \neq 0$, the equilibrium point is saddle hyperbolic.

In the case of a two-dimensional dynamic system as

$$\dot{x} = f(x, \alpha), \;\; x = (x_1, x_2)^{\mathrm{T}} \in \mathbb{R}^2, \tag{2}$$

with smooth f and an equilibrium point of $x_0 = 0$, $\mathbf{A}$ has two eigenvalues λ_1 and λ_2. There are three topological categories for hyperbolic equilibrium points of a two-dimensional system: stable foci (nodes), saddles, and unstable foci (nodes). Foci and nodes are topologically equivalent and can be simply identified based on eigenvalues. Stable equilibrium points have two-dimensional stable manifolds without any unstable manifold; these conditions are vice versa for unstable equilibrium points. Saddle equilibrium points have one-dimensional stable and unstable manifolds. There are two conditions where the equilibrium point is not hyperbolic. In the first case, for some values of α, a simple real eigenvalue is close to zero and $\lambda_1 = 0$, which is called fold bifurcation. In the second case, a couple of simple complex eigenvalue is close to the imaginary axis and $\lambda_{1,2} = j\omega_0$ with $\omega_0 > 0$, that is called Hopf bifurcation. In this paper, the latter case is adopted in the proposed strategy.

2) Hopf Bifurcation: Consider the continuous-time parameter-dependent two-dimensional system as

$$\begin{cases} \dot{x_1} = \alpha x_1 - x_2 - x_1(x_1^2 + x_2^2), \\ \dot{x_2} = x_1 + \alpha x_2 - x_2(x_1^2 + x_2^2). \end{cases} \tag{3}$$

For all α values, this system has the equilibrium point $x_1 = x_2 = 0$. This system always has the equilibrium point at the origin. For $\alpha < 0$, this point is a stable focus while for $\alpha > 0$, it is an unstable focus. For the critical value of $\alpha = 0$, the equilibrium at origin is nonlinearly stable. In this system, supercritical Hopf bifurcation occurs.

For the system with the opposite sign as

$$\begin{cases} \dot{x_1} = \alpha x_1 - x_2 + x_1(x_1^2 + x_2^2), \\ \dot{x_2} = x_1 + \alpha x_2 + x_2(x_1^2 + x_2^2), \end{cases} \tag{4}$$

the equilibrium stability at origin for $\alpha \neq 0$ is the same as system (3), while the equilibrium for $\alpha = 0$ is nonlinearly unstable. In this system, the subcritical Hopf bifurcation occurs. This system has an unstable limit cycle that vanishes when α crosses zero and being positive.

3) Basic Principle of the Proposed Method: Regarding the insignificant change in the current of LVDC microgrids during high-resistance faults, the fault current signal can be considered as a weak signal. Following the above discussion, a fault condition can be discriminated from a normal one by adopting the parameter-dependent differential equation of (1) is considered as the fault detection criterion that it is in subcritical Hopf bifurcation condition. Therefore, by changing α, until these changes are due to interference and measurement errors, the equilibrium is asymptotically stable. However, when a short-circuit fault occurs, phase portraits tend to infinity exponentially; it increases the fault detection speed significantly. It should be noted that the radius of the limit cycle determines the maximum interference and measurement

This article has been accepted for publication in a future issue of this journal, but has not been fully edited. Content may change prior to final publication. Citation information: DOI 10.1109/JESTPE.2019.2961903, IEEE Journal of Emerging and Selected Topics in Power Electronics

errors. In this case, the variable of DC microgrid current can be considered as the bifurcation parameter in this dynamic system. The adopted dynamic system is stable during normal operating conditions while it is unstable during a short-circuit fault. In the latter condition, phase portraits move towards infinity and adopted tool can make a significant difference between fault and normal conditions. In this paper, the PFHO differential equations set is adopted as the protective decision-making tool. The harmonic oscillator as a simple and linear oscillator can properly distinguish a stable condition from an unstable one. The variation of fault current as the PFHO parameter can change the phase portrait from the oscillatory stable state to the unstable state.

B. Analysis of Periodically-Forced Harmonic Oscillator

The second-order differential equation of PFHO is expressed as [20]

$$\ddot{y} + p\dot{y} + qy = \cos(\omega t), \tag{5}$$

where p and q are equation constants. ω is the angular frequency. The general solution of (5) can be expressed as

$$y(t) = N(t) + F(t), \tag{6}$$

where N is the general solution of the unforced equation while F is the particular solution of the forced equation. The unforced form of harmonic oscillator equation is

$$\ddot{y} + p\dot{y} + qy = 0. \tag{7}$$

Considering $x_1 = y$ and $x_2 = \dot{y}$, one can write

$$\begin{cases} \dot{x_1} = \dot{y} = x_2, \\ \dot{x_2} = \ddot{y} = -p\dot{y} - qy = -qx_1 - px_2. \end{cases} \tag{8}$$

The state matrix of state-space representation is expressed as

$$\mathbf{A} = \begin{pmatrix} 0 & 1 \\ -q & -p \end{pmatrix} \tag{9}$$

Thus, the eigenvalues of characteristic equation of (7) are

$$\lambda_{1,2} = \frac{-p \pm \sqrt{p^2 - 4q}}{2}. \tag{10}$$

The state of harmonic oscillator depends on p and q values. As shown in Fig. 1, there are four stable states and two unstable states as follows.

If $\lambda_1 < \lambda_2 < 0$, the oscillator state is overdamped with the solution of

$$N(t) = c_1 e^{\lambda_1 t} + c_2 e^{\lambda_2 t}, \tag{11}$$

where c_1 and c_2 are arbitrary constants.

If one eigenvalue is in the form of $\alpha + j\beta$ with the negative real part and positive imaginary part, the oscillator state is underdamped with the solution of

$$N(t) = c_1 e^{\alpha t}\cos(\beta t) + c_2 e^{\alpha t}\sin(\beta t). \tag{12}$$

If one eigenvalue is in the form of $j\beta$ ($p = 0$) with $\beta > 0$, the oscillator state is undamped with the solution of

$$N(t) = c_1 \cos(\beta t) + c_2 \sin(\beta t). \tag{13}$$

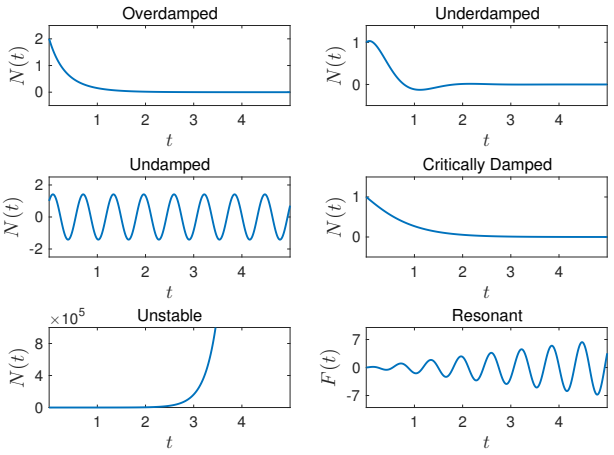

Fig. 1. Various states of harmonic oscillator.

If $\lambda_1 = \lambda_2 = \lambda < 0$, the oscillator state is critically damped with the solution of

$$N(t) = c_1 e^{\lambda t} + c_2 t e^{\lambda t}. \tag{14}$$

If $p < 0$, both eigenvalues are in the right-hand side of complex plane and thus, the harmonic oscillator is unstable.

The forced response of (5) is

$$F(t) = a\cos(\omega t) + b\sin(\omega t), \tag{15}$$

where

$$a = \frac{q - \omega^2}{(p\omega)^2 + (q - \omega^2)^2}, \quad b = \frac{p\omega}{(p\omega)^2 + (q - \omega^2)^2}. \tag{16}$$

If $p = 0$ and $q = \omega^2$, the oscillator state is resonant with the forcing response of

$$F(t) = t\big(a\cos(\omega t) + b\sin(\omega t)\big). \tag{17}$$

C. PFHO Based Protection Strategy

The operating principle of the proposed PFHO based protection is to change the system state during a fault condition by adding small turbulence. The main feature of PFHO is that when the system state changes to chaotic motion (positive real eigenvalue), the system becomes unstable and its state variable suddenly increases to infinity. This promising feature makes PFHO a proper choice for fault detection in LVDC microgrids. It facilitates fault detection because independent of study microgrid structure/topology, the PFHO state variable is either infinity (during fault condition) or non-infinity (during normal operation). The remainder of this subsection is dedicated to the mathematical description of the proposed scheme.

Using a current transducer, the first step of the proposed strategy is to measure the line current. The proposed scheme relies on IEDs at both ends of the protected zone, processing the current measurements. The filtered current measurement is sampled using the IED. Then, it is normalized as

$$i_{\mathrm{IED}}^{\mathrm{pu}}[k] = \frac{i[k]}{I_{\mathrm{base}}}, \tag{18}$$

where k is the sampling step and $i_{\mathrm{IED}}^{\mathrm{pu}}$ and I_{base} are the normalized IED current and base current, respectively.

This article has been accepted for publication in a future issue of this journal, but has not been fully edited. Content may change prior to final publication. Citation information: DOI 10.1109/JESTPE.2019.2961903, IEEE Journal of Emerging and Selected Topics in Power Electronics

To address the bidirectional current flow and low fault current of weak fault conditions, the superimposed component of current is commonly calculated. This component poses the fault signature and can be calculated using the superposition theorem [21]. The fault current component $i^{\text{pu}}_{\text{IED,F}}$ can be assumed as the sum of normal-running $i^{\text{pu}}_{\text{IED,N}}$ and superimposed $i^{\text{pu}}_{\text{IED,SI}}$ currents. Thus, $i^{\text{pu}}_{\text{IED,SI}}$ can be calculated as

$$i^{\text{pu}}_{\text{IED,SI}}[k] = i^{\text{pu}}_{\text{IED,F}}[k] - i^{\text{pu}}_{\text{IED,N}}[k]. \tag{19}$$

To calculate the superimposed component, the Delta filter [22] is used as

$$i^{\text{pu}}_{\text{IED,SI}}[k] = i^{\text{pu}}_{\text{IED}}[k] - i^{\text{pu}}_{\text{IED}}[k - k_d], \tag{20}$$

where k_d is the number of Delta filter time delay samples. The promising feature of superimposed component is that during normal operation, it is zero while when a disturbance occurs, it changes instantaneously.

Using the superimposed component of current, the PFHO equation is expressed as

$$\ddot{y} + p'\dot{y} + qy = \cos(\omega t), \tag{21}$$

where

$$p' = p + k_{\text{amp}} \cdot i^{\text{pu}}_{\text{IED,SI}}, \tag{22}$$

and k_{amp} is the amplifier gain.

In the proposed protection scheme, each protected zone is equipped with two IEDs at its both ends. These IEDs calculate the state variable of the PFHO equation. During normal operation, the PFHO system is kept in one of the four stable states. By adopting $p = 1$ and $q = 0.5$, the eigenvalues of system (7) becomes $\lambda_{1,2} = -0.5 \pm 0.5j$; thus, the N is underdamped during normal condition, as stated in Subsection II-B. By considering $c_1 = c_2 = 1$, and $\omega = 1$, and solving (5), the PFHO state is oscillatory stable and the peak value of y is equal to 1.45. This peak value is independent of study microgrid because it is the output of PFHO. During normal operation when the superimposed current is nearly zero, $p' \simeq p = 1$ and thus, the system state is in stable mode. When a fault occurs, the sign of superimposed current determines whether the system motion is normal or chaotic.

During normal operation, the current direction at both ends is the same. When a fault occurs inside the zone (internal fault), the current direction depends on the severity of fault condition. If the fault path resistance is high, the current direction at both ends does not change during the fault. As shown in Fig. 2(a), however, the superimposed current direction changes independent of fault severity. The superimposed components of current at sending and receiving ends are calculated as

$$\begin{cases} i^{\text{pu,send}}_{\text{IED,SI}} = i^{\text{pu,send}}_{\text{IED,F}} - i^{\text{pu,send}}_{\text{IED,N}} = +i_{\text{fault}}, \\ i^{\text{pu,receive}}_{\text{IED,SI}} = i^{\text{pu,receive}}_{\text{IED,F}} - i^{\text{pu,receive}}_{\text{IED,N}} = -i_{\text{fault}}, \end{cases} \tag{23}$$

where i_{fault} is the fault current.

Fig. 2(b) shows that for the case of forward and reverse external faults, the superimposed components of current at both ends are expressed as

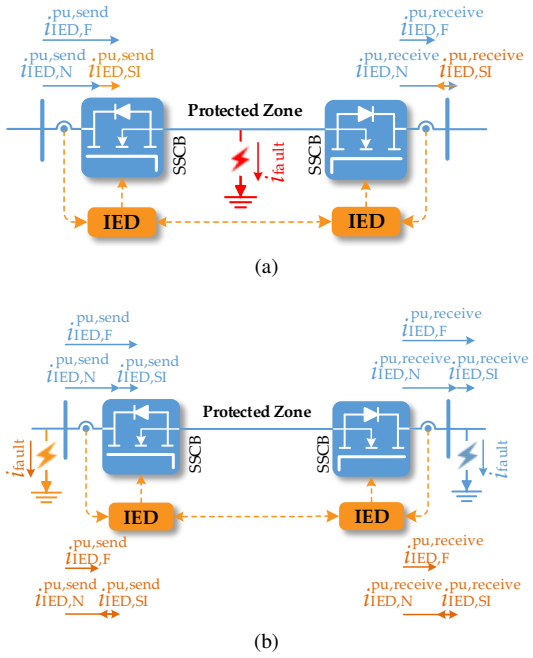

Fig. 2. Current components during normal and fault conditions. (a) Internal fault and (b) external forward and reverse faults.

$$\begin{cases} i^{\text{pu,send}}_{\text{IED,SI}} = i^{\text{pu,receive}}_{\text{IED,SI}} = +i_{\text{fault}}, & \text{forward fault} \\ i^{\text{pu,send}}_{\text{IED,SI}} = i^{\text{pu,receive}}_{\text{IED,SI}} = -i_{\text{fault}}, & \text{reverse fault.} \end{cases} \tag{24}$$

Consequently, in the case of an internal fault, the state variable y calculated at receiving end increases to infinity because $p' < 0$ and based on (10), the eigenvalues of PFHO move to right-hand side of complex plane and the system becomes unstable, while its peak at sending end is lower than 2 because of $p' > 0$. However, in the cases of external faults, the system state at both ends remains in normal motion for a forward fault or it falls into the chaotic motion and y reaches infinity for a reverse fault. It should be noted that for a fault with very high resistance where the fault current change is negligible, p' remains positive and the system does not become unstable; however, such faults require special protection measures which is out of the scope of this paper. The PFHO based directional element $\mathbb{D}_{\text{PFHO}}$ is defined as

$$\mathbb{D}_{\text{PFHO}} = \begin{cases} 0, & y < 2 \\ 1, & \text{otherwise.} \end{cases} \tag{25}$$

The IEDs of each zone exchange the information of the proposed directional element through the communication link. If $\mathbb{D}_{\text{PFHO}}$ at both ends is the same, this condition is interpreted as a normal or an external fault condition. However, different $\mathbb{D}_{\text{PFHO}}$ values at both ends indicates an internal fault; in this condition, the faulty zone IEDs send the trip signal to their associated solid-state circuit breakers (SSCBs) for isolating this zone from the healthy ones.

In the case of SSCB failure, the adjacent SSCBs should be opened. To this end, if an IED sends the open command to its associated SSCB and after a certain time delay, the fault current is still non-zero, it sends an SSCB failure message

This article has been accepted for publication in a future issue of this journal, but has not been fully edited. Content may change prior to final publication. Citation information: DOI 10.1109/JESTPE.2019.2961903, IEEE Journal of Emerging and Selected Topics in Power Electronics

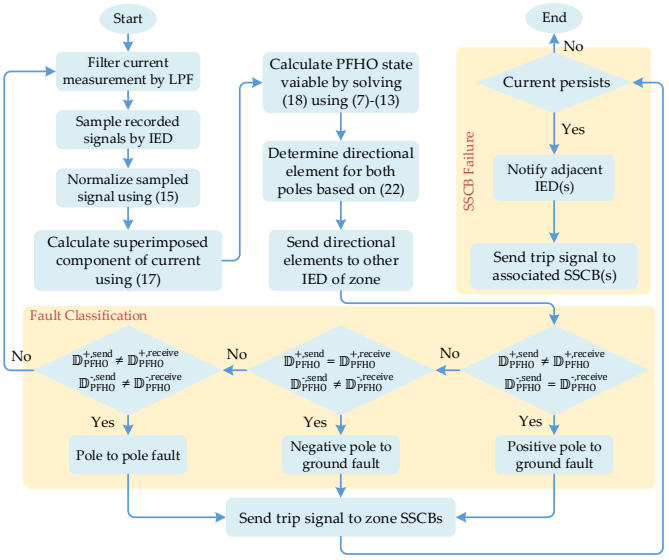

Fig. 3. Flowchart of the proposed PFHO based directional protection strategy.

to adjacent IEDs at the same bus and they will trip their associated SSCBs immediately.

D. Flowchart of the Proposed Algorithm

The flowchart of the proposed protection scheme is shown in Fig. 3. The filtered current signal is processed by the IED to calculate its superimposed component. Then, the PFHO equation is formed using this component and its state variable is calculated at both ends. Based on this variable, the developed directional element is determined and its information is sent to the IED located at another end of the protected zone. It should be noted that the directional element should be determined for both poles for the detection of both positive pole to ground and negative pole to ground faults. As shown in the Fault Classification section of Fig. 3, the PG and PP faults can be classified based on positive pole $\mathbb{D}^{+}_{\mathrm{PFHO}}$ and negative pole $\mathbb{D}^{-}_{\mathrm{PFHO}}$ directional elements at sending and receiving ends. When a fault is detected and the trip command is sent to the faulty zone SSCBs, the current is still monitored. If the fault current persists for a certain time, the fault zone IED notifies its adjacent IED(s) to trip adjacent SSCB(s) at the same bus, as shown in the SSCB Failure section of Fig. 3.

E. Speed of Proposed Scheme

To protect the network equipment against DC microgrid fault current with high magnitude and rate of change, each severe fault should be isolated from the DC microgrid during few milliseconds [13]. The amplifier gain affects the speed of the proposed scheme. Increment of k_{amp} increases the rate of change of p', speeding up the system change to unstable mode. However, a high k_{amp} results in malfunction of the proposed method for normal small disturbances in line current signal. In the developed scheme, k_{amp} is adopted equal to 2000.

From the delay point of view, the high bandwidth fiber optic communication reduces the queuing and transmission delays

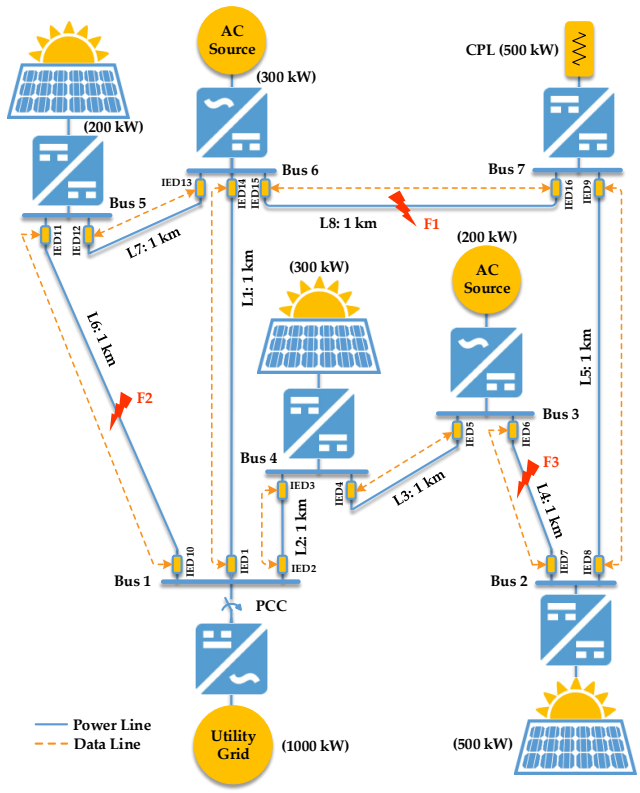

Fig. 4. Test meshed LVDC microgrid network.

to around 0.1 ms [13]. Also, using advanced routing, the processing delay can be reduced to a few microseconds. Since the microgrid lines are commonly short, the propagation delay is in the order of a few microseconds. On the other hand, SSCBs can interrupt a DC fault within a few microseconds [23]. It ensures high speed of the proposed scheme.

III. Study LVDC Microgrid

Fig. 4 shows the single-line diagram of the study meshed LVDC microgrid [6]. The structure of this microgrid is similar to the distribution part of the IEEE 14-bus system. This 8-bus microgrid includes three photovoltaic (PV) sources and two AC sources. The study microgrid is interfaced with the AC utility grid through a three-phase three-level voltage-sourced inverter (VSI). The bus 7 includes a resistive load supplied from the microgrid through a DC-DC buck converter as a constant power load (CPL). The operating voltage of the study microgrid is $\pm$750 V. The study microgrid includes 8 lines with a length of 1 km where the cable resistance and inductance are 0.017 Ω/km and 3.3 mH/km, respectively. It is a 3-wire system (bipolar) and is equipped with the TN-S grounding scheme, connecting the converter midpoint to the ground.

The study microgrid can operate in both grid-connected and islanded modes. In the former mode, the VSI is controlled using the external and internal control loops; the DC-link voltage is regulated by the former loop while the real and reactive components of the grid current are controlled using the latter loop. The PV systems consist of 305.2 W SunPower modules that are interfaced with the microgrid through the

This article has been accepted for publication in a future issue of this journal, but has not been fully edited. Content may change prior to final publication. Citation information: DOI 10.1109/JESTPE.2019.2961903, IEEE Journal of Emerging and Selected Topics in Power Electronics

boost converters. In the grid-connected mode, the boost converter is controlled by the maximum power point tracking algorithm while in the islanded mode, it is controlled by the droop based multi-loop control system [24]. Each AC source is integrated with the microgrid through an AC-DC rectifier and a DC-DC converter. In the islanded mode, DC-DC converter is controlled by the multi-loop control system while in the grid-connected mode, the current reference of the current control loop is set by the microgrid management system. It should be noted that the current reference of DC-DC converters is limited to two times the nominal current of each converter to protect the semiconductor switches.

IV. Performance Evaluation

The developed scheme is evaluated by performing several case studies in the MATLAB/Simulink environment. The sampling frequency of IED and k_d are adopted equal to 10 kHz and 1000, respectively. The base power and voltage for perunit calculations are equal to 1000 kW and 1500 V, respectively.

A. Case 1: Bolted PP Fault in Grid-Connected Mode

In the first case study, a bolted PP fault is simulated at the middle of line L8 (F1 in Fig. 4) in the grid-connected mode of operation at $t = 5$ s. Fig. 5 shows the simulation results from IEDs 15 and 16. This severe fault condition increases the sending end line current to 10 times the base current. The second row of this figure shows that the superimposed component of current before the fault condition is zero while after the fault occurrence, the calculated superimposed currents by IEDs 15 and 16 change to about +5.5 pu and -1.5 pu, respectively. It results in p' decreases below zero in the receiving end while the positive sign of $i^{\text{pu}}_{\text{IED15,SI}}$ keeps p' beyond zero. Consequently, the system state at the sending end is normal motion while it is the chaotic motion at the receiving end, as shown in the third row of Fig. 5. The fourth row of the figure shows that during the normal condition, the maximum of PFHO state variable y is lower than 2; when the fault occurs, it increases to infinity at receiving end while it is still below 2 at sending end. The proposed PFHO directional element at receiving end changes to 1 at about 5.0001 s while it does not change at sending end. Considering the processing, communication, propagation, and SSCB operation delays, the fault detection time is about 400 μs that is well shorter than the required fault detection time of few milliseconds for DC microgrids. Table I presents the PFHO state variable calculated by IEDs of healthy lines where both system states of each line are either equal to infinity or smaller than 2. Thus, the related IEDs do not interpret this disturbance as an internal fault.

B. Case 2: High-Resistance PG Fault in Grid-Connected Mode

The second case study is dedicated to evaluating the developed protection algorithm in the case of high-resistance faults in the grid-connected operating mode. For this purpose, a negative pole-to-ground fault with fault resistance of 30 Ω is simulated at point F2 in Fig. 4 at $t = 5$ s. The simulation

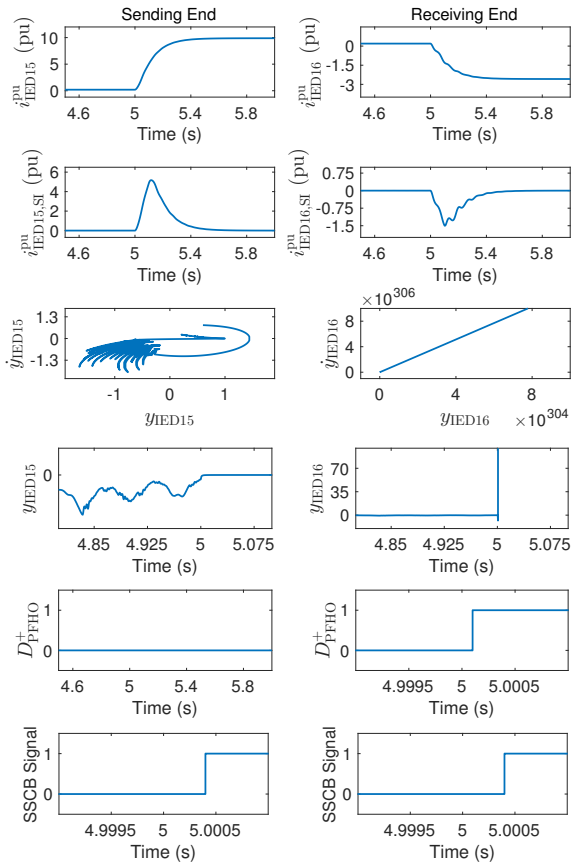

Fig. 5. Performance of the proposed PFHO based protection scheme during a bolted fault in grid-connected operating mode.

TABLE I
PFHO State Variable for Healthy Lines in Case 1

Line Number	Sending End	Receiving End
L1	$y_{\text{IED1}} < 2$	$y_{\text{IED14}} < 2$
L2	$y_{\text{IED2}} = \infty$	$y_{\text{IED3}} = \infty$
L3	$y_{\text{IED4}} = \infty$	$y_{\text{IED5}} = \infty$
L4	$y_{\text{IED6}} = \infty$	$y_{\text{IED7}} = \infty$
L5	$y_{\text{IED8}} = \infty$	$y_{\text{IED9}} = \infty$
L6	$y_{\text{IED10}} < 2$	$y_{\text{IED11}} < 2$
L7	$y_{\text{IED12}} < 2$	$y_{\text{IED13}} < 2$

results from IEDs 10 and 11 for both positive and negative poles are shown in Fig. 6. Since the healthy positive pole is not affected by the fault, the superimposed current at both ends is zero. Thus, the PFHO state variable remains lower than 2, preserving the stable mode at both ends. In this condition, the associated SSCBs of these IEDs at positive pole remain closed, as shown in the third row of Fig. 6. This weak fault condition does not result in current direction change and it changes the superimposed currents of sending and receiving ends only to +0.03 pu and -0.018 pu, respectively. However, the PFHO equation enters unstable mode at receiving end while it remains in stable mode at sending end. The associated SSCBs of the negative pole are opened at 5.009 ms by IEDs 10 and 11. Thus, the proposed method properly classifies this event as a negative pole-to-ground fault. Although the overall fault detection time is slightly longer than 4 ms, the fault

This article has been accepted for publication in a future issue of this journal, but has not been fully edited. Content may change prior to final publication. Citation information: DOI 10.1109/JESTPE.2019.2961903, IEEE Journal of Emerging and Selected Topics in Power Electronics

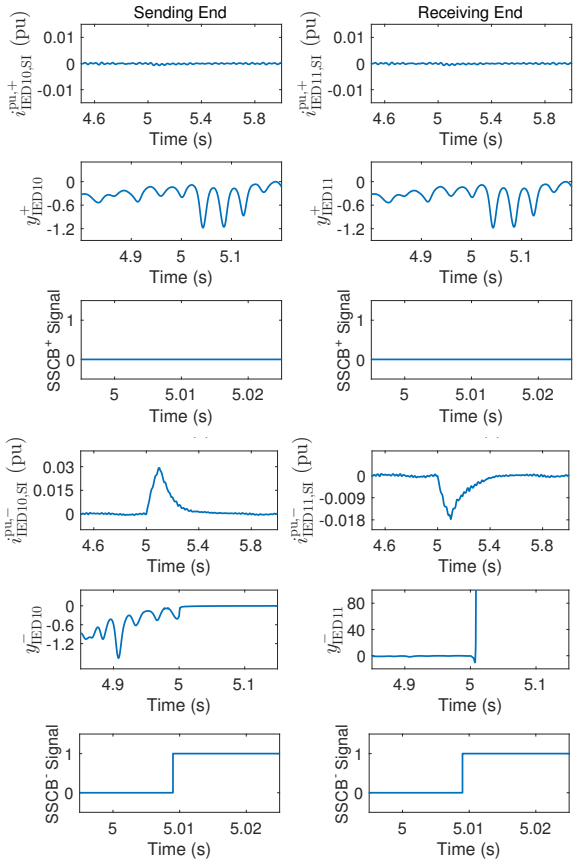

Fig. 6. Performance of the proposed PFHO based protection scheme during a high-resistance fault in grid-connected operating mode.

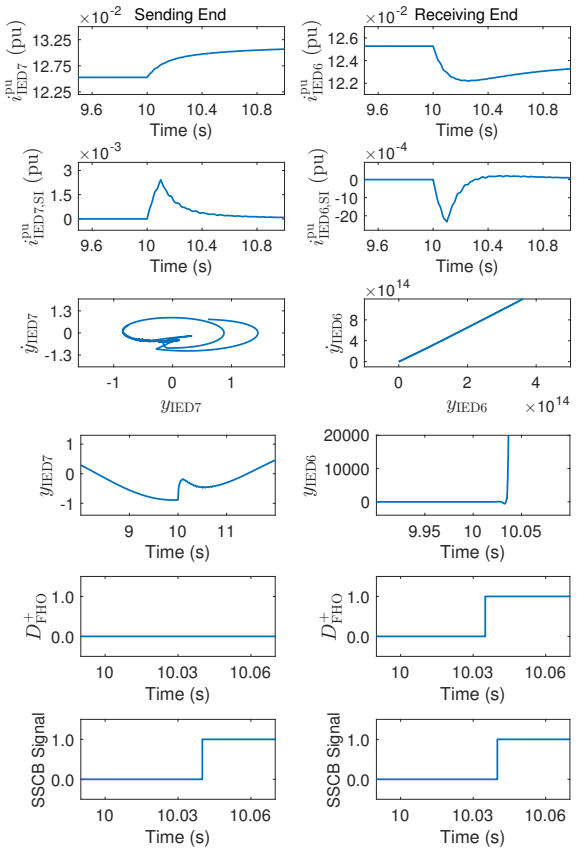

Fig. 7. Performance of the proposed PFHO based protection scheme during a high-resistance fault in islanded operating mode.

current is very limited in this case and is not harmful.

C. Case 3: High-Resistance PP Fault in Islanded Mode

The performance of the protection strategies in an islanded LVDC microgrid is rarely investigated. The third scenario aims to evaluate the effectiveness of the proposed protection scheme in the islanded mode of operation. To this end, the point of common coupling (PCC) switch is opened and the microgrid is controlled using the droop control. A high-resistance PP fault with fault resistance of 200 Ω in the line L4 (F3 in Fig. 4) at $t = 10$ s makes this scenario a challenging condition. Fig 7 shows the simulation results from IEDs 6 and 7. No current direction change and low superimposed current at both ends are evident in the first and second rows of this figure, respectively. However, p' decreases to -3.4 at receiving end that causes the associated PFHO state variable reaches infinity, while this variable is less than 2 in another end. The overall fault detection time is 39 ms.

D. Comparative Assessment

To make a comparison between the proposed protection scheme and superimposed based protection strategies, a PG fault is simulated at F1. The fault detection time in MSPG calculated using superimposed current [18] is about 2 ms while the superimposed transient energy based protection strategy proposed in [17] detects this fault after about 5 ms. However, the fault detection time of the proposed strategy is about 700 μs which verifies the effectiveness of the proposed protection strategy. On the other hand, Table II compares the features of the proposed protection strategy and unit protection schemes reviewed in Section I. In addition to evaluating the performance for bolted and high-resistance PP and PG faults and consisting of a fault classification scheme, the proposed strategy is evaluated in both grid-connected and islanded modes of operation and does not require threshold calculation for different microgrid structures/topologies.

V. Conclusion

This paper has proposed a unit protection scheme for meshed LVDC microgrids. In this scheme, each line is equipped with two IEDs at both ends, processing the current measurements. Each IED calculates the superimposed component of current as the additive input of the PFHO equation and communicates with the IED at another end of the protected zone for fault detection and with the adjacent IED(s) in the event of SSCB failure. In the case of a reverse fault that the superimposed current is negative, the PFHO state variable increases to infinity while the positive superimposed current in the case of a forward fault keeps the oscillator in stable mode, preserving the PFHO state variable lower than 2. The two-state value of the PFHO state variable eliminates the need for proper protection threshold selection in different microgrid structures/topologies. The proposed scheme effectively protects

TABLE II
COMPARISON BETWEEN PROPOSED STRATEGY AND SOME EXISTING UNIT PROTECTION SCHEMES

	[13]	[14]	[15]	[16]	[17]	[18]	Proposed
Are both PP and PG faults considered?	No	Yes	Yes	No	No	Yes	Yes
Is fault classification considered?	No	No	No	No	No	Yes	Yes
Is high-resistance fault considered?	No	Yes	Yes	Yes	Yes	Yes	Yes
Are both grid-connected and islanded modes of operation considered?	No	No	No	No	No	No	Yes
Is no threshold calculation required?	No	No	No	No	No	No	Yes

both grid-connected and islanded LVDC microgrids without the change of protection settings. Several case studies on a meshed LVDC microgrid show that a bolted fault is isolated by the developed periodically-forced harmonic oscillator based strategy in less than 500 μs while it can determine the faulty zone with the fault path resistance of 200 Ω in less than 40 ms, verifying the speed and sensitivity of the proposed scheme.

REFERENCES

[1] S. Beheshtaein, R. M. Cuzner, M. Forouzesh, M. Savaghebi, and J. M. Guerrero, "DC microgrid protection: A comprehensive review," *IEEE J. Em. Sel. Top. P.*, accepted for publication, 2019.

[2] S. D. A. Fletcher, P. J. Norman, S. J. Galloway, and G. M. Burt, "Analysis of the effectiveness of non-unit protection methods within DC microgrids," in *IET Conference on Renewable Power Generation*, Sept. 2011.

[3] J. Yang, J. E. Fletcher, and J. O'Reilly, "Short-circuit and ground fault analyses and location in VSC-based DC network cables," *IEEE Trans. Ind. Electron.*, vol. 59, no. 10, pp. 3827–3837, Oct. 2012.

[4] P. Cairoli and R. A. Dougal, "Fault detection and isolation in medium-voltage DC microgrids: Coordination between supply power converters and bus contactors," *IEEE Trans. Power Electron.*, vol. 33, no. 5, pp. 4535–4546, May 2018.

[5] M. E. Baran and N. R. Mahajan, "Overcurrent protection on voltage-source-converter-based multiterminal DC distribution systems," *IEEE Trans. Power Del.*, vol. 22, no. 1, pp. 406–412, Jan. 2007.

[6] K. A. Saleh, A. Hooshyar, and E. F. El-Saadany, "Hybrid passive-overcurrent relay for detection of faults in low-voltage DC grids," *IEEE Trans. Smart Grid*, vol. 8, no. 3, pp. 1129–1138, May 2017.

[7] A. Meghwani, S. C. Srivastava, and S. Chakrabarti, "A new protection scheme for DC microgrid using line current derivative," in *IEEE Power Energy Society General Meeting*, Jul. 2015.

[8] ——, "A non-unit protection scheme for DC microgrid based on local measurements," *IEEE Trans. Power Del.*, vol. 32, no. 1, pp. 172–181, Feb. 2017.

[9] J. D. Park, J. Candelaria, L. Ma, and K. Dunn, "DC ring-bus microgrid fault protection and identification of fault location," *IEEE Trans. Power Del.*, vol. 28, no. 4, pp. 2574–2584, Oct. 2013.

[10] S. D. A. Fletcher, P. J. Norman, K. Fong, S. J. Galloway, and G. M. Burt, "High-speed differential protection for smart DC distribution systems," *IEEE Trans. Smart Grid*, vol. 5, no. 5, pp. 2610–2617, Sept. 2014.

[11] S. Dhar, R. K. Patnaik, and P. K. Dash, "Fault detection and location of photovoltaic based DC microgrid using differential protection strategy," *IEEE Trans. Smart Grid*, vol. 9, no. 5, pp. 4303–4312, Sep. 2018.

[12] S. Dhar and P. K. Dash, "Differential current-based fault protection with adaptive threshold for multiple PV-based DC microgrid," *IET Renew. Power Gen.*, vol. 11, no. 6, pp. 778–790, 2017.

[13] A. A. S. Emhemed, K. Fong, S. Fletcher, and G. M. Burt, "Validation of fast and selective protection scheme for an LVDC distribution network," *IEEE Trans. Power Del.*, vol. 32, no. 3, pp. 1432–1440, Jun. 2017.

[14] R. Mohanty and A. K. Pradhan, "Protection of smart DC microgrid with ring configuration using parameter estimation approach," *IEEE Trans. Smart Grid*, vol. 9, no. 6, pp. 6328–6337, Nov. 2018.

[15] ——, "DC ring bus microgrid protection using the oscillation frequency and transient power," *IEEE Syst. J.*, vol. 13, no. 1, pp. 875–884, Mar. 2019.

[16] ——, "A superimposed current based unit protection scheme for DC microgrid," *IEEE Trans. Smart Grid*, vol. 9, no. 4, pp. 3917–3919, Jul. 2018.

[17] R. Mohanty and A. K. Pradhan, "Protection of DC and hybrid AC-DC microgrids with ring configuration," in *7th International Conference on Power Systems*, Pune, India, Dec. 2017.

[18] M. Salehi, S. A. Taher, I. Sadeghkhani, and M. Shahidehpour, "A poverty severity index-based protection strategy for ring-bus low-voltage DC microgrids," *IEEE Trans. Smart Grid*, vol. 10, no. 6, pp. 6860–6869, Nov. 2019.

[19] Y. Kuznetsov, *Elements of Applied Bifurcation Theory*, 2nd ed. Springer-Verlag New York, 1998.

[20] S. F. Ellermeyer, "The periodically—forced harmonic oscillator," [Online]. Available: http://ksuweb.kennesaw.edu/ sellerme//sfehtml/classes/math3310/fho.pdf, 2003.

[21] M. A. Zamani, A. Yazdani, and T. S. Sidhu, "A communication-assisted protection strategy for inverter-based medium-voltage microgrids," *IEEE Trans. Smart Grid*, vol. 3, no. 4, pp. 2088–2099, Dec. 2012.

[22] G. Benmouy and J. Roberts, "Superimposed quantities: Their true nature and application in relays, schweitzer engineering laboratories," *Inc. Pullman, WA USA, SEL USA*, 1999.

[23] A. A. S. Emhemed and G. M. Burt, "An advanced protection scheme for enabling an LVDC last mile distribution network," *IEEE Trans. Smart Grid*, vol. 5, no. 5, pp. 2602–2609, Sept. 2014.

[24] J. Guerrero, J. Vasquez, J. Matas, L. de Vicuña, and M. Castilla, "Hierarchical control of droop-controlled AC and DC microgrids—a general approach toward standardization," *IEEE Trans. Ind. Electron.*, vol. 58, no. 1, pp. 158–172, Jan. 2011.